ACS OMEGA

http://pubs.acs.org/journal/acsodf

Article

Lignin Nanoparticles as Sustainable Photoprotective Carriers for Sunscreen Filters

Davide Piccinino, Eliana Capecchi, Valentina Trifero, Elisabetta Tomaino, Claudia Marconi, Alessandra Del Giudice, Luciano Galantini, Stefano Poponi, Alessandro Ruggieri, and Raffaele Saladino*

Cite This: *ACS Omega* 2022, 7, 37070−37077

Read Online

ACCESS | Metrics & More | Article Recommendations | Supporting Information

ABSTRACT: Sunscreen filters may be degraded after prolonged UV exposure with loss of their shielding property and generation of harmful radical species. They are contained in cosmetic formulations in high concentrations, so the improvement of photostability is of relevance for safety concerns. We report here that lignin nanoparticles are sustainable carriers and photostabilizers of two common UV chemical filters, namely, avobenzone and octyl methoxycinnamate. These compounds have been encapsulated by nanoprecipitation into kraft lignin nanoparticles using eco-certified dimethyl isosorbide as a primary solvent and deionized water as an antisolvent. After the encapsulation, both compounds significantly prolonged the half-life stability against UV irradiation. The stabilizing properties of lignin nanoparticles were further improved by coencapsulation of avobenzone and octyl methoxycinnamate with hydroxytyrosol, a natural phenol with antioxidant activity recovered from olive oil wastes and characterized by skin regenerative properties.

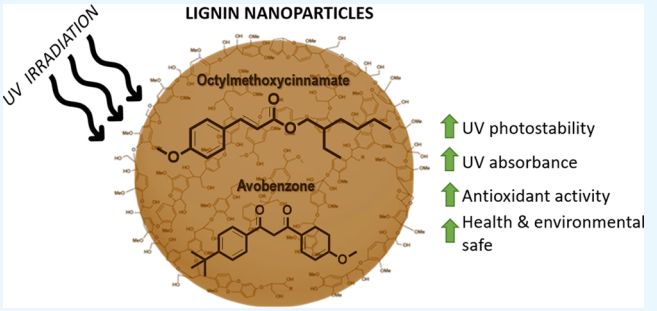

INTRODUCTION

UV sunscreen filters (SSFs) commonly found in commercial formulations may cause production of radical species after prolonged irradiation with a concomitant loss of cosmetic function and emergence of toxicity.[1−3] Photostabilizers are used to avoid these side effects by quenching the high-energy excited states of SSFs,[4] but in turn, they can be degraded with production of toxic side products.[5,6] Over the past few years, photostabilizers from renewable sources received a great interest due to green chemistry and circular economy concerns.[7] Lignin, the most abundant polyphenol in nature, is a waste recovered from pulp and paper and biorefinery processes.[8] It is characterized by different beneficial properties for cosmetic applications, including antioxidant activity,[9] sun protection factor booster,[10] antimicrobial,[11] and metal chelating effects.[12] In addition, lignin forms stable colloidal nanoparticles (LNPs) deprived of toxicity[13] and characterized by high UV absorbing capacity and radical scavenging properties[14] as a consequence of the formation of π-interaction between the aromatic subunits of the polymer.[15] Examples of application of native lignin and LNPs as sunscreens are reviewed,[16,17] and the role played by these nanodevices in the formulation of cosmetic and cosmeceutic products is deeply investigated.[18,19] These properties associated with the presence of an internal cavity make LNPs a suitable nanodevice for the encapsulation and stabilization of active substances in drug delivery[20] and Pickering emulsion technologies.[21] Here, we report that LNPs from kraft lignin are efficient and sustainable carriers for the stabilization of two common SSFs,[22] 4-*tert*-butyl-4′-methoxydibenzoylmethane **1** (avobenzone) and 2-ethylhexyl-3-(4-methoxyphenyl)prop-2-enoate **5** (octyl methoxycinnamate). Compound **1** is a largely applied UV-A filter whose photostability is dependent on the overall composition of the formulate.[23] Conversely, **5** is a highly active and photolabile UV-B filter.[24] Under prolonged irradiation, compound **1** is subjected to α-cleavage by a McLafferty-like retro-heteroene hydrogen rearrangement to yield *tert*-butylbenzene **2**, 4-*tert*-butyl benzoic acid **3**, and *para*-methoxy benzoic acid **4** (Figure 1, panel A).[25] The allergenic effect and cytotoxicity of **2**−**4** at the lymph node level are reported.[26] In a similar way, the prolonged irradiation of **5** causes isomerization to (*Z*)-*cis* counterpart **6**, followed by side chain degradation to 4-methoxy benzaldehyde **7** and 2-ethylhexanol **8**, or alternately, [2 + 2]π cycloaddition to cyclobutane dimers **9a**,**b** (Figure 1, panel B).[27−29]

Toxic effects of **6**, **7**, and **9a**,**b** against cellular viability in NIH/3T3 mouse fibroblast cells are reported.[30] Antioxidants

Received: April 6, 2022
Accepted: August 9, 2022
Published: October 10, 2022

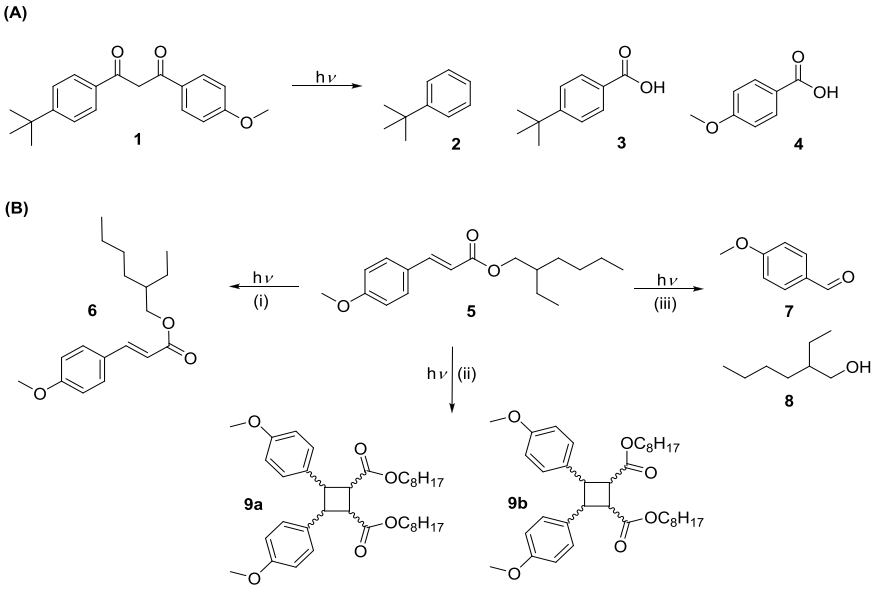

Figure 1. Photodegradation pathway of **1** (panel A) and **5** (panel B) after UV irradiation. (i) *Z*/*E* isomerization process; (ii) side chain cleavage; and (iii) [2 + 2]π cycloaddition.

have been explored and applied as energy quenchers[31] in order to improve the photostability of **1** and **5**.[32,33] These compounds are not completely deprived of toxicity since they can generate radical oxygen species and reactive quinone derivatives.[33,34] Presently, few examples of the application of LNPs as carriers for UV filters are reported, apart from encapsulation of titanium dioxide with consequent decreased photoactivity[35] and the Pickering emulsions with SSF oils.[36] These procedures involve the formation of emulsions in which the UV filter is surrounded by LNPs, or alternately, a coating of a titanium dioxide core by layer-by-layer deposition. Otherwise, examples of encapsulation of UV filters in the internal cavity of LNPs are not reported, despite that these nanodevices are expected to improve the stability of the active ingredients by acting as a UV barrier, contemporaneously favoring their controlled release in the medium.[37] Here, we describe the encapsulation of **1** and **5** into LNPs by nanoprecipitation using eco-certified dimethyl isosorbide (DMI) as a primary solvent and deionized water as an anti-solvent. High values of loading capacity (LC) and loading efficacy (LE) were obtained. Compounds **1** and **5** were also coencapsulated with *para*-hydroxy phenethyl alcohol **10** (hydroxytyrosol), a natural phenol from olive wastewater, characterized by high antioxidant activity and beneficial skin regenerative effects,[38] usually applied in cosmetic formulations and functional food.[39−41] Compound **10** was selected due to its well-known UV-B shielding capacity and radical quenching properties.[42] After the loading procedure, compounds **1** and **5** showed increased photostability with respect to the bare counterpart, showing a beneficial role of the lignin carrier and hydroxytyrosol in the inhibition of photodegradative pathways.

MATERIALS AND METHODS

Reagents. 4-*Tert*-butyl-4′-methoxydibenzoylmethane **1** (avobenzone), 2-ethylhexyl-3-(4-methoxyphenyl)prop-2-enoate **5** (octyl methoxycinnamate, and *para*-hydroxy phenethyl alcohol **10** (hydroxytyrosol) were obtained from Sigma-Aldrich and used without further purification. Kraft lignin (KL) was obtained from Sigma-Aldrich and was purified before use by standard procedures,[43] including alkali−acid treatment and continuous washing with deionized water. DMI (purity 98.0%) was purchased from TCI Europe and used without further purification.

Encapsulation Protocol and Determination of Loading Parameters. LNPs were prepared using the nanoprecipitation method. KL (100.0 mg) was dissolved in DMI:H_2O (3.0 mL, 2.5:0.5 v/v) at 50 °C for 12 h under gentle magnetic stirring. Milli-Q water (6.0 mL) was added to the KL solution and LNPs formed instantaneously. For the encapsulation procedure, the appropriate compound to be encapsulated (0.06 mmol) was dissolved in the KL solution before the addition of water. A similar procedure was repeated in the presence of a mixture of compounds (1:1 molar ratio). After the precipitation, LNPs were recovered by centrifugation (6500 rpm, 10 min). The LC and LE were evaluated using the high-performance liquid chromatography (HPLC) analysis of the supernatant obtained after centrifugation using eqs 1 and 2:

$$\text{LC (\%)} : \frac{(\text{weight of starting SSF} - \text{weight of unloaded SSF})}{\text{weight of lignin}} \times 100 \quad (1)$$

$$\text{LE (\%)} : \frac{(\text{weight of starting SSF} - \text{weight of unloaded SSF})}{\text{weight of starting SSF}} \times 100 \quad (2)$$

Here, LC is the percentage of the encapsulated compound with respect to starting KL, while LE represents the amount of encapsulated compound with respect to the initial concentration of SSF.

2,2′-Diphenyl picrylhydrazyl (DPPH) Radical Scavenging Activity. The antioxidant activity of LNPs was evaluated by the DPPH radical scavenging assay. The test was performed starting from different amounts of LNPs (500, 250,

https://doi.org/10.1021/acsomega.2c02133
ACS Omega 2022, 7, 37070−37077

Scheme 1. General Procedure for the Preparation and Characterization of Loaded LNPs

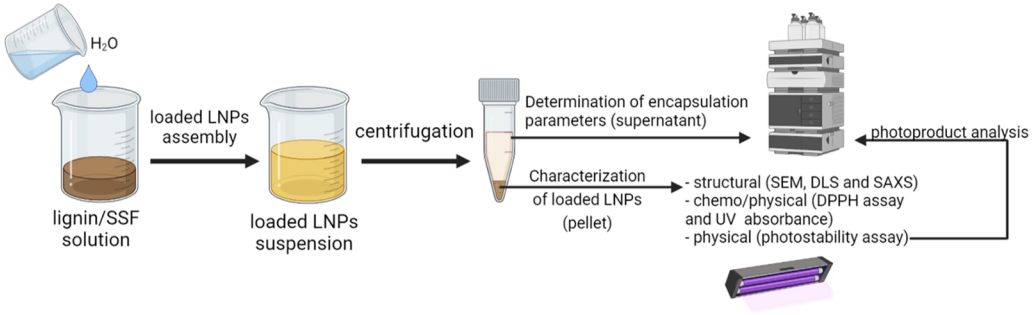

100, 50, and 10 μg/mL) in H_2O (0.550 mL), which were added to a freshly prepared DPPH solution (2.45 mL, 0.7 mM in MeOH). The spectrophotometric analysis was carried out in duplicate at 25 °C. The radical scavenging activity was monitored as a function of time by measuring the absorbance band of DPPH at 517 nm (λ_{max}) until the absorbance values reached a plateau. The kinetics of the process was analyzed for each concentration tested, and the amount of DPPH remaining at the steady state was estimated. This value was used to calculate the IC_{50} (concentration of the substrate that causes 50% loss of DPPH activity). Data were expressed as percentage of inhibition of DPPH activity based on the following eq 3:

$$\text{inhibition of DPPH (\%)}: \frac{(\text{Abs control} - \text{Abs sample})}{\text{Abs control}} \times 100 \quad (3)$$

where "Abs control" is the absorbance of the DPPH solution in the absence of the sample.

Hydrodynamic Diameter and ζ-Potential Analyses. The hydrodynamic diameter and ζ-potential values were evaluated in H_2O by dynamic light scattering (DLS) using a Zetasizer Nano ZS (Malvern Instruments, Malvern, UK) apparatus equipped with a He−Ne laser (633 nm, fixed scattering angle of 173°, 25 °C). Measurements were performed in triplicate at 25 °C.

Field-Emission Scanning Electron Microscopy (FESEM). FESEM was carried out using a ZEISS Gemini 500 (Oberkochen, Germany) at 5 kV. As a general procedure, LNPs in water (20 μL) were deposited on a coverslip coated with gold (AGAR auto sputter coater) and dehydrated in air. The coverslip was mounted on the stub with conductive carbon glue and a thin film (5.0 nm) of chromium was deposited using the Sputter Quorum Q150T ES plus to make the sample sufficiently conductive for measurement purposes.

Small-Angle X-ray Scattering (SAXS). The measurements were performed by SAXS with a Xeuss 2.0 Q-Xoom system (Xenocs SAS, Grenoble, France) equipped with a microfocus Genix 3D X-ray source (λ = 0.1542 nm) and a two-dimensional Pilatus3 R 300K detector, which can be placed at a variable distance from the sample. The beam size was determined by the two-pinhole collimation system equipped with "scatterless" slits to be 0.5 mm × 0.5 mm. Calibration of the scattering vector q range is described in eq 4

$$q: \frac{(4\pi^* \sin\theta)}{\lambda} \quad (4)$$

and 2θ is the scattering angle, and the calibration was performed using silver behenate. Measurements with two different sample detector distances (26.2 and 250 cm) were performed and the overall explored q region was $0.045 < q < 17$ nm^{-1}. Samples of LNPs (concentration of the SAXS samples: 1.0 mg/mL) dispersed in a DMI:H_2O 1:3 mixture were inserted into disposable borosilicate glass capillaries with a nominal internal diameter of 0.15 cm, sealed with hot glue, and placed in the instrument sample chamber at room temperature and reduced pressure (~0.2 mbar). The two-dimensional scattering patterns were measured for a total of 3.5 h acquisition time per sample, subtracted for the "dark" counts, and then masked, azimuthally averaged, and normalized for calculating the transmitted beam intensity, exposure time, and subtended solid angle per pixel using the FoxTrot software developed at SOLEIL. The one-dimensional I versus q profiles were then subtracted for the solvent and capillary contributions and expressed in absolute scale units (cm^{-1}) by dividing for the sample thickness estimated by scanning the capillary with the X-ray beam. The different angular ranges were merged using the SAXS utilities tool.[44]

UV−Visible Assay. LNPs (10 μg) in cyclohexane were analyzed in a quartz cuvette (3.0 mL, 1 cm path length) by a Varian Cary UV 60 scan (Crawley, UK) in the range between 250 and 800 nm with a scan speed of 400 nm/min and a bandwidth of 5 nm at 25 °C under gentle stirring. The analysis was elaborated by the UV−vis scan software.

Photostability Assay. LNPs (10.0 mg) were suspended in cyclohexane (5.0 mL) in an open glass lens (10.0 cm diameter). The suspension was irradiated using a UV Hg low-pressure lamp (HAERUS 250W; 40 cm of distance to obtain 3000 mj/cm^2) for 20.0 min. After the irradiation, tetrahydrofuran (THF, 5.0 mL) was added to the crude in order to degrade LNPs, followed by filtration (25 mm, 0.22 μm syringe filter), roto-evaporation, and freeze-drying. The percentage of photodegradation was evaluated by HPLC analysis of the supernatant after the filtration step.

HPLC Analysis. The HPLC analysis was performed using an UltiMate 3000 rapid resolution system (Thermo Fisher Scientific) equipped with an Alltima C18 column (250 mm × 4.6 mm, 5 μm), an injection volume of 10 μL, a mobile phase flow rate of 1.0 mL/min, and a detector set up at 319 nm for **1**, 361 nm for **5**, and 280 nm for **10**, respectively. The analysis was repeated in triplicate. The compounds were separated using the isocratic method using 95.0% MeOH and 5.0% ultrapure formic acid for 25 min and quantified using the calibration curve method.

RESULTS AND DISCUSSION

Preparation and Characterization of LNPs. LNPs were prepared by nanoprecipitation using eco-certified DMI as the

https://doi.org/10.1021/acsomega.2c02133
ACS Omega 2022, 7, 37070−37077

primary solvent and deionized H_2O as the anti-solvent. As a general procedure, compounds **1** and **5** (0.06 mmol) were dissolved in DMI/water (3.0 mL, 2.5:0.5 v/v) in the presence of KL (100 mg) at 50 °C under gentle magnetic stirring. Deionized water (6.0 mL) was added with formation of a colloidal suspension of LNPs and contemporaneous encapsulation of the selected compound. The mixture was centrifuged (7000 rpm, 15 min), washed with deionized water (×3, 9.0 mL), and freeze-dried to yield LNPs-**1** and LNPs-**5**, respectively (Scheme 1).

A similar procedure was applied in the presence of a mixture of **1** and **5** (1:1 molar ratio) to yield LNPs-**1**/**5**. In addition, compounds **1** and **5** were coencapsulated with hydroxytyrosol **10** (0.06 mmol) to yield LNPs-**1**/**10** and LNPs-**5**/**10**, respectively. LC (eq 1) and LE (eq 2) of LNPs were evaluated by HPLC analysis of the residual compound in the supernatant after the centrifugation step. Irrespective of the experimental conditions, the LNPs showed high values of LE and LC (Table 1), confirming the efficacy of LNPs in the encapsulation of aromatic derivatives.[45]

Table 1. Encapsulation Parameters, Hydrodynamic Diameter, ζ-Potential, and Polydispersive Index of LNPs-1, LNPs-5, LNPs-1/5, LNPs-1/10, and LNPs-5/10

entry	sample	compound	LE (%)	LC (%)	ζ-potential	mean size (nm)	PDI[a]
1	LNPs				−34.5	225	0.101
2	LNPs-**1**	**1**	86.1	10.8	−33.7	291	0.141
3	LNPs-**5**	**5**	79.7	12.4	−32.9	286	0.139
4	LNPs-**1/5**	**1,5**	82.9	11.1	−34.1	301	0.138
5	LNPs-**1/10**	**1,10**	85.1	12.0	−36.0	302	0.134
6	LNPs-**5/10**	**5,10**	81.9	10.9	−34.2	297	0.135

[a]Polydispersive index.

Figure 2 shows the FESEM analysis results of LNPs-**1** (panel A), LNPs-**5** (panel B), and LNPs-**1**/**5** (panel C) as selected representative samples (SEM images of empty LNPs, LNPs-**1**/**10**, and LNPs-**5**/**10** are shown in Figure S1, Supporting Information). The samples were characterized by regular and

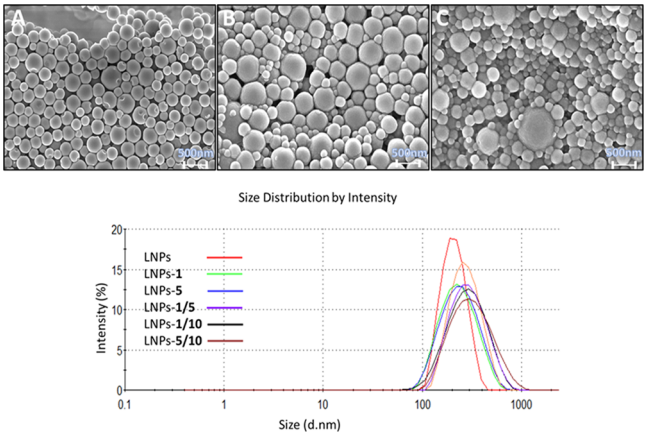

Figure 2. Results of (top) FESEM analysis of LNPs-**1** (panel A), LNPs-**5** (panel B), and LNPs-**1**/**5** (panel C) and (bottom) DLS analysis.

spherical-shaped nanoparticles bearing small clumps on the surface, which appears rather rough. DLS analysis of LNPs showed the formation of monodisperse population of particles (Figure 2, bottom).

The average diameter of LNPs was in the range between 286 nm (LNPs-**5**; entry 3, Table 1) and 302.3 nm (LNPs-**1**/**10**; entry 5, Table 1). It was higher than that previously observed for empty LNPs (entry 1, Table 1) in accordance with the steric hindrance of encapsulated compounds.[46] The ζ-potential value was found to be almost constant irrespective of the loaded compound (Table 1, entries 2−6) and of the same order of magnitude as empty LNPs (Table 1, entry 1), confirming the absence of significant adsorption phenomena on the surface of LNPs.

The SAXS analysis was performed in the selected cases of empty LNPs, LNPs-**1**, LNPs-**5**, and LNPs-**1**/**5**. As shown in Figure 3 panel A, the four samples had almost superimposable

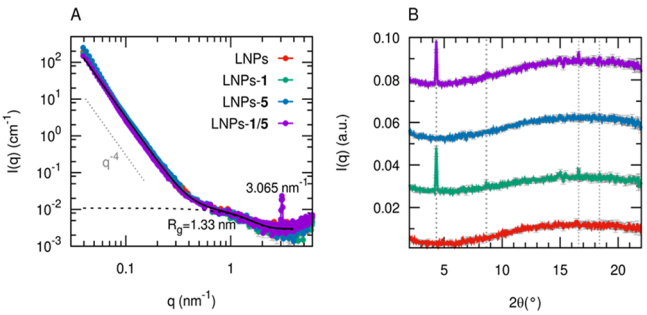

Figure 3. SAXS profiles of LNP samples. (A) The intensity vs q data in a double logarithmic scale are shown as colored dots and lines (LNPs, red; LNPs-**1**, green; LNPs-**5**, blue; and LNPs-**1**/**5**, purple), while the model function of the Porod law decay (c/q^4, with $c = 3.2 \times 10^{-4}$ cm^{-1} nm^{-4}, reference slope indicated as dotted gray line) and the Guinier contribution ($I(0)\exp(-R_g^2 q^{2/3})$ with $I(0) = 8 \times 10^{-3}$ cm^{-1} and $R_g = 1.33$ nm) with a flat background (3×10^{-3} cm^{-1}) are shown as a solid black line. The latter contribution is also reported as a dashed black line. The most evident diffraction peak position is indicated. (B) The wider-angle scattering region presenting the diffraction peaks for samples LNPs-**1** and LNPs-**1**/**5** (q > nm^{-1}) is highlighted by plotting data as a function of 2θ rather than q. The data are vertically shifted on the intensity scale for better visualization and the peak positions are indicated by dotted gray lines.

scattering profiles, but LNPs-**1** and LNPs-**1**/**5** showed additionally the presence of an evident diffraction peak at 3.065 nm^{-1}, corresponding to an interplanar distance of 2.05 nm, and subsequent weaker peaks (the second at 6.13 nm^{-1}) characteristic of a crystalline phase. These peaks were not observed in LNPs-**5** and in empty LNPs. Considering the reported crystallinity of compound **1** (compound **5** is an oil) and comparing the observed positions of the diffraction peaks in units of 2θ (at 4.3, 8.6, 16.6, and 18.4°, Figure 3 panel B) to those reported in the literature,[47] these data suggest the presence of compound **1** in LNPs-**1** and LNPs-**1**/**5** samples, respectively, in the crystalline isoform II, reported as a metastable phase accessible from the melt of the commercially available form I.

Regarding the measured scattering signal at lower angles, in agreement with the DLS data showing LNPs with diameters of the order of 200−300 nm, the overall size of the particles in the samples lies beyond the resolution limit of the used SAXS. Therefore, the decay of the initial intensity in the scattering profiles (q <0.4 nm^{-1}) is evident on a length scale between 70

https://doi.org/10.1021/acsomega.2c02133
ACS Omega 2022, 7, 37070−37077

and 10 nm, following the power law (Porod law, $\sim 1/q^4$), expected for the interface between the particles and the solvent. A fit according to the Guinier law in this region provides such additional feature, related to a radius of gyration R_g of 1.33 nm, which means sizes of 3−4 nm (from the value of the radius of gyration R_g of 1.33 nm estimated from the intensity decay according to the Guinier law) such an additional feature could be interpreted as due to both the characteristic internal porosity of the self-assembled LNPs and the individual lignin units.[15,48]

UV-Shielding Capacity of LNPs. The UV-shielding capacity of LNPs-**1**, LNPs-**5**, and LNPs-**1**/**5** was evaluated by a spectrophotometric analysis after dispersion of 10 μg of the particles in 3.0 mL of cyclohexane (250−800 nm) at 25 °C (UV-shielding data of LNPs-**1**/**10** and LNPs-**5**/**10** are shown in Figure S2).

Empty LNPs and compounds **1**, **5**, and **10** were used as references (Figure 4, panels A−C). LNPs-**1**, LNPs-**5**, and

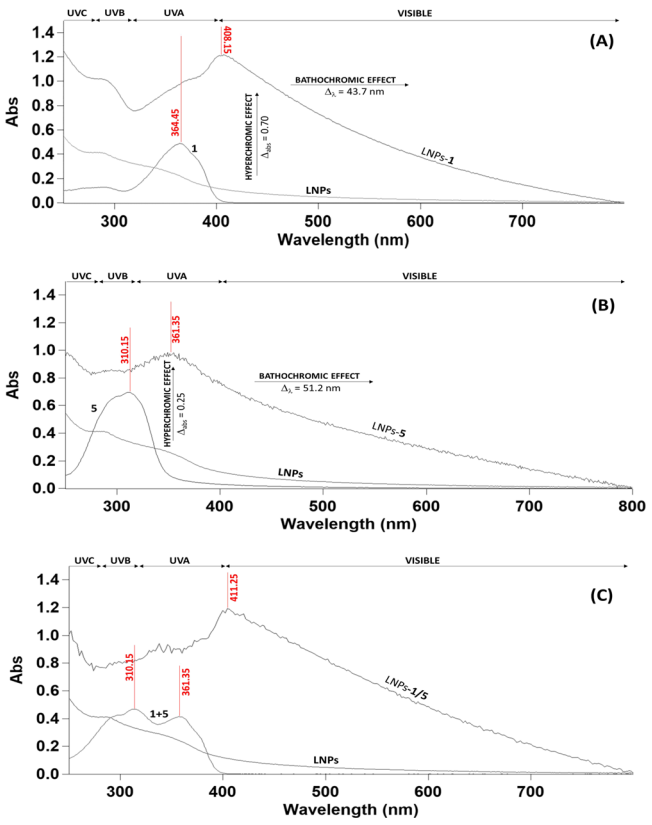

Figure 4. In vitro UV−vis absorbance of aqueous suspensions of LNPs-**1** (panel A), LNPs-**5** (panel B), and LNPs-**5**/**10** (panel C).

LNPs-**1**/**5** showed increased absorption capacity (hyperchromic effect) and pronounced bathochromic shift with respect to references. In particular, LNPs-**1** and LNPs-**5** showed an appreciable red shift ($\Delta\lambda$ of 43.7 nm and $\Delta\lambda$ of 51.2 nm, respectively) with respect to the corresponding references **1** (364.5 nm) and **5** (310.2 nm) as reported in Figure 4 panels A and B. A similar effect was observed for LNPs **1**/**5** (Figure 4, panel C).

This effect was probably due to the interaction between the auxo-chromic groups of KL and the chromophore moieties of compound **1** and **5**, associated with the formation of typical J-aggregation modes in lignin subunits.

Antioxidant Activity of LNPs. The antioxidant activity of LNPs-**1**, LNPs-**5**, LNPs-**1**/**5**, LNPs-**1**/**10**, and LNPs-**5**/**10** was evaluated by measuring the radical scavenging activity against DPPH. The percentage of quenching of the DPPH radical was evaluated at different sample concentrations by applying eq 3. The IC_{50} values (μg/mL of sample that causes 50% loss of DPPH concentration) are reported in Figure 5 and Table S1. Empty LNPs and commercially available butyl-hydroxytoluene (BHT) were used as references. LNPs-**5** and LNPs-**1**/**5** showed higher antioxidant activities than LNPs-**1** and references. The presence of **10** further increased the antioxidant activity, and LNPs-**1**/**10** and LNPs-**5**/**10** showed IC_{50} values lower than those of LNPs-**1** and LNPs-**5**, respectively.

LNPs-**5**/**10** showed the highest antioxidant activity. Irrespective of the sample, the antioxidant activity of LNPs was probably due to the radical scavenging properties of aromatic OH moieties, as previously reported.[49]

UV Photostability of 1 and 5 after Encapsulation into LNPs. The ability of LNPs to protect **1** and **5** from UV photodegradation was evaluated by analysis of the residual amount of these compounds after irradiation. Briefly, LNPs **1** and **5** (10 mg) were suspended in 5.0 mL of cyclohexane and irradiated by a UV lamp (Hg, low pressure) for 20 min at 25 °C. The irradiation of **1** and **5** alone or their mixture (1:1 equivalent ratio) was performed under similar experimental conditions as a reference. After the irradiation of the sample, the nanoparticles were treated with THF (5.0 mL) in order to deliver the encapsulated compounds. The residual amount of **1** and **5** was determined after evaporation of the organic phase by HPLC analysis. High percentage of photodegradation was measured for **1** (72.2%) and **5** (79.1%) as references with formation of expected photoproducts **2**−**4** and **7** and **8**, respectively. The percentage of photodegradation increased for **5** (87.8%) and decreased for **1** (69.2%) during the irradiation of the mixture due to the undesired photochemical-induced isomerization of **5** by **1**.[50,51] It is worth noting that photodegradation was significantly reduced in the case of LNPs-**1** (12.8%) and LNPs-**5** (10.9%), confirming the photostability of the compounds after the encapsulation process (Figure 6 and Table S2). A similar result was observed for LNPs-**1**/**5** in which case the energy transfer process was limited by the presence of lignin. This enhanced photostability is of great commercial interest since both **1** and **5** are widely used as a mixture in sunscreen formulations. Finally, the photodegradation of **1** and **5** was further inhibited by the presence of **10** (LNPs-**1**/**10** 5.1% and LNPs-**5**/**10** 4.2%) as a consequence of a combined UV shielding and antioxidant effect exerted by this catechol derivative (Figure 6 and Table S2).

CONCLUSIONS

Photolabile UV filters avobenzone and octyl methoxycinnamate have been successfully encapsulated into lignin nanoparticles by a sustainable and efficient nanoprecipitation procedure using eco-certified DMI as the primary solvent and deionized water as the anti-solvent. The loaded nanoparticles were isolated in high yield and were characterized by high values of LC and LE. FESEM and DLS analyses confirmed the formation of spherical particles with a size (between 286 and 302 nm) slightly higher than the empty counterpart as a consequence of the steric hindrance of loaded compounds. The ζ-potential values were found to be

https://doi.org/10.1021/acsomega.2c02133
ACS Omega 2022, 7, 37070−37077

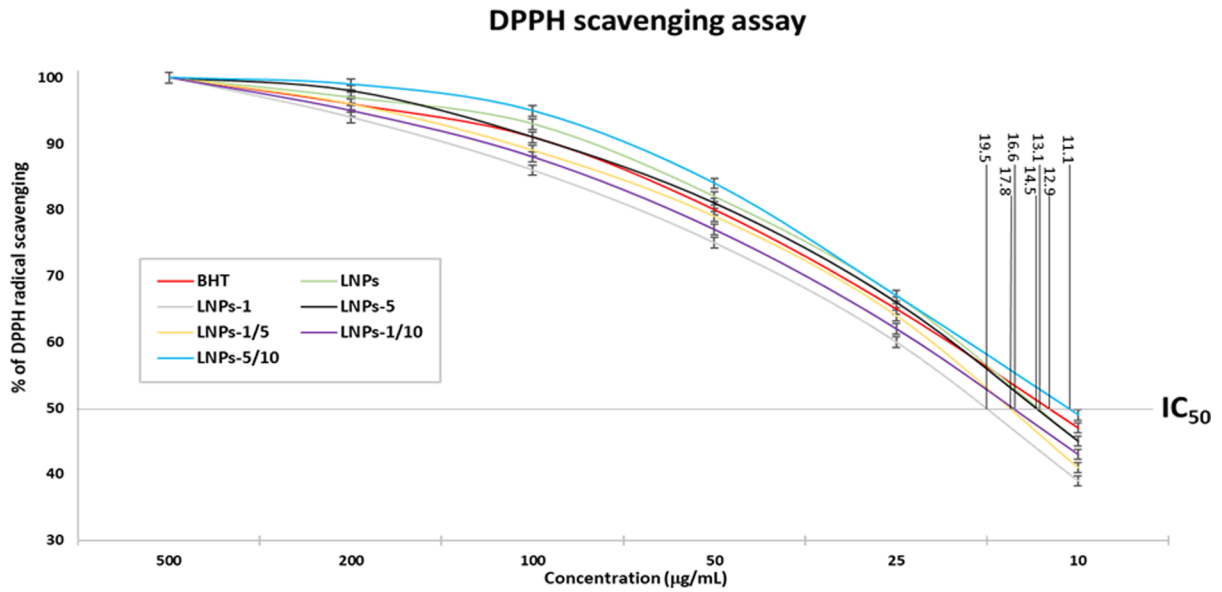

Figure 5. DPPH scavenging activity of loaded lignin nanoparticles presented as % of DPPH radical inhibitions and IC_{50} values (μg/mL).

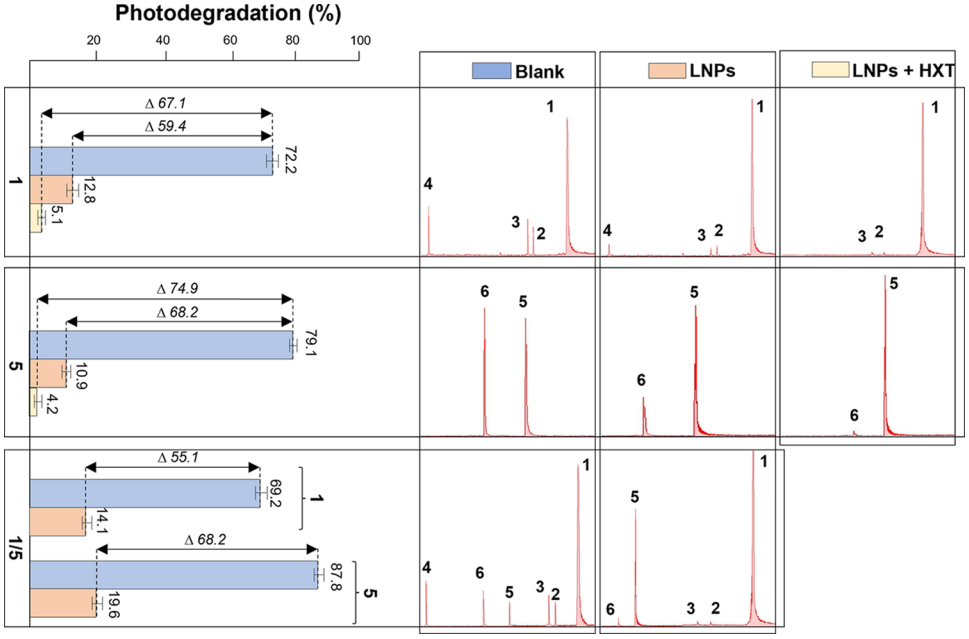

Figure 6. Photostability evaluation of loaded LNPs compared to the corresponding dissolved SSF.

unchanged after the loading procedures in accordance with the absence of a significant adsorption process on the surface of particles. The loaded lignin nanoparticles generally increased the UV−vis absorption capacity with respect to references, with the presence of bathochromic and hyperchromic effects suggesting the occurrence of interactions between the auxochromic groups of lignin and the chromophore moieties in selected chemical filters. In addition, the loaded lignin nanoparticles showed IC_{50} antioxidant values comparable to commercially available antioxidants like BHT as a reference. The key role of lignin nanoparticles in enhancing photostability of selected compounds was finally demonstrated by the significant inhibition of degradative processes, even when the two compounds were tested in a 1:1 ratio mixture. In this latter case, the presence of hydroxytyrosol further increased the photostability of the compounds, allowing the design of more safe, effective, and eco-sustainable SSFs.

■ ASSOCIATED CONTENT

Supporting Information

The Supporting Information is available free of charge at https://pubs.acs.org/doi/10.1021/acsomega.2c02133.

SEM images of LNPs, LNPs-1/10, and LNPs-5/10 (Figure S1), UV-shielding properties of LNPs-1/10 and LNPs-5/10 (Figure S2), IC_{50} values obtained from the DPPH assay (Table S1), and photodegradation and photostabilization values of SSFs before and after encapsulation into lignin nanoparticles (Table S2) (PDF)

https://doi.org/10.1021/acsomega.2c02133
ACS Omega 2022, 7, 37070−37077

AUTHOR INFORMATION

Corresponding Author

Raffaele Saladino − *Department of Ecological and Biological Sciences, University of Tuscia, 01100 Viterbo, Italy;* orcid.org/0000-0002-4420-9063; Email: saladino@unitus.it

Authors

Davide Piccinino − *Department of Ecological and Biological Sciences, University of Tuscia, 01100 Viterbo, Italy*

Eliana Capecchi − *Department of Ecological and Biological Sciences, University of Tuscia, 01100 Viterbo, Italy;* orcid.org/0000-0002-5448-0658

Valentina Trifero − *Department of Ecological and Biological Sciences, University of Tuscia, 01100 Viterbo, Italy*

Elisabetta Tomaino − *Department of Ecological and Biological Sciences, University of Tuscia, 01100 Viterbo, Italy*

Claudia Marconi − *Department of Chemistry, University of Rome La Sapienza, 00185 Rome, Italy*

Alessandra Del Giudice − *Department of Chemistry, University of Rome La Sapienza, 00185 Rome, Italy;* orcid.org/0000-0002-1916-8300

Luciano Galantini − *Department of Chemistry, University of Rome La Sapienza, 00185 Rome, Italy;* orcid.org/0000-0001-5484-2658

Stefano Poponi − *Department of Economics, Engineering, Society, and Enterprise, University of Tuscia, 01100 Viterbo, Italy*

Alessandro Ruggieri − *Department of Economics, Engineering, Society, and Enterprise, University of Tuscia, 01100 Viterbo, Italy*

Complete contact information is available at: https://pubs.acs.org/10.1021/acsomega.2c02133

Funding

The reported study was jointly funded by ECOSUN (T0002E0001) and LIOO (85F21000550002) "Laboratory of innovation of the olive oil supply chain" (FISR project).

Notes

The authors declare no competing financial interest.

ABBREVIATIONS

LNPs, lignin nanoparticles; SSF, sunscreen filters; AVOB, avobenzone; OMC, octyl methoxycinnamate; HXT, hydroxytyrosol; DPPH, 2,2′-diphenyl picrylhydrazyl radical

REFERENCES

(1) Nash, J. F.; Tanner, P. R. Relevance of UV filter/sunscreen product photostability to human safety. *Photodermatol., Photoimmunol. Photomed.* **2014**, *30*, 88−95.

(2) Ahmed, M. B.; Johir, M. A. H.; Zhou, J. L.; Ngo, H. H.; Guo, W. S.; Sornalingam, K. Photolytic and photocatalytic degradation of organic UV filters in contaminated water. *Curr. Opin. Green Sustainable Chem.* **2017**, *6*, 85−92.

(3) Maier, H.; Schauberger, G.; Martincigh, B. S.; Brunnhofer, K.; Honigsmann, H. Ultraviolet protective performance of photoprotective lipsticks: change of spectral transmittance because of ultraviolet exposure. *Photodermatol., Photoimmunol. Photomed.* **2005**, *21*, 84−92.

(4) Benevenuto, C. G.; Di Matteo, M. A. S.; Campos, P. M. B. G. M.; Gaspar, L. R. Influence of the Photostabilizer in the Photoprotective Effects of a Formulation Containing UV-Filters and Vitamin A. *Photochem. Photobiol.* **2010**, *86*, 1390−1396.

(5) Fu, P. P.; Xia, Q. S.; Yin, J. J.; Cherng, S. H.; Yan, J.; Mei, N.; Chen, T.; Boudreau, M. D.; Howard, P. C.; Wamer, W. G. Photodecomposition of vitamin a and photobiological implications for the skin. *Photochem. Photobiol.* **2007**, *83*, 409−424.

(6) Butt, S. T.; Christensen, T. Toxicity and phototoxicity of chemical sun filters. *Radiat. Prot. Dosim.* **2000**, *91*, 283−286.

(7) Franca, C. C. V.; Ueno, H. M. Green cosmetics: perspectives and challenges in the context of green chemistry. *Desenvolv. Meio Ambiente* **2020**, *53*, 133−150.

(8) Haile, A.; Gelebo, G. G.; Tesfaye, T.; Mengie, W.; Mebrate, M. A.; Abuhay, A.; Limeneh, D. Y. Pulp and paper mill wastes: utilizations and prospects for high value-added biomaterials. *Bioresour. Bioprocess.* **2021**, *8*, 35.

(9) Garcia, A.; Amendola, D.; Gonzalez, M.; Spigno, G.; Labidi, J. Lignin as Natural Radical Scavenger. Study of the Antioxidant Capacity of Apple Tree Pruning Lignin Obtained by Different Methods. *Chem. Eng. Trans.* **2011**, *24*, 925.

(10) Piccinino, D.; Capecchi, E.; Delfino, I.; Crucianelli, M.; Conte, N.; Avitabile, D.; Saladino, R. Green and Scalable Preparation of Colloidal Suspension of Lignin Nanoparticles and Its Application in Eco-friendly Sunscreen Formulations. *ACS Omega* **2021**, *6*, 21444−21456.

(11) Alzagameem, A.; Klein, S. E.; Bergs, M.; Do, X. T.; Korte, I.; Dohlen, S.; Huwe, C.; Kreyenschmidt, J.; Kamm, B.; Larkins, M.; Schulze, M. Antimicrobial Activity of Lignin and Lignin-Derived Cellulose and Chitosan Composites against Selected Pathogenic and Spoilage Microorganisms. *Polymers* **2019**, *11*, 670.

(12) Ruthran, V. B.; Barman, P.; Kadam, R.; Kumar, A. Lignin-based adsorbent for effective removal of toxic heavy metals from wastewater. *Emergent Mater.* **2022**, *5*, 923−943.

(13) Stine, J. S.; Harper, B. J.; Conner, C. G.; Velev, O. D.; Harper, S. L. In Vivo Toxicity Assessment of Chitosan-Coated Lignin Nanoparticles in Embryonic Zebrafish (Danio rerio). *Nanomaterials* **2021**, *11*, 111.

(14) Piccinino, D.; Capecchi, E.; Botta, L.; Bizzarri, B. M.; Bollella, P.; Antiochia, R.; Saladino, R. Layer-by-Layer Preparation of Microcapsules and Nanocapsules of Mixed Polyphenols with High Antioxidant and UV-Shielding Properties. *Biomacromolecules* **2018**, *19*, 3883−3893.

(15) Bao, D. D.; Xie, Y. T.; Ma, S. L.; Wu, Z. B.; Piao, J. G.Self-assembly of a renewable lignin biopolymer in nanoparticles with multiple morphologies. *J. Appl. Polym. Sci.***2019**, *136* (), DOI: 10.1002/app.47482.

(16) Tran, M. H.; Phan, D. P.; Lee, E. Y. Review on lignin modifications toward natural UV protection ingredient for lignin-based sunscreens. *Green Chem.* **2021**, *23*, 4633−4646.

(17) Lee, S. C.; Yoo, E.; Lee, S. H.; Won, K. Preparation and Application of Light-Colored Lignin Nanoparticles for Broad-Spectrum Sunscreens. *Polymers* **2020**, *12*, 699.

(18) Ratanasumarn, N.; Chitprasert, P. Cosmetic potential of lignin extracts from alkaline-treated sugarcane bagasse: Optimization of extraction conditions using response surface methodology. *Int. J. Biol. Macromol.* **2020**, *153*, 138−145.

(19) Gordobil, O.; Olaizola, P.; Banales, J. M.; Labidi, J. Lignins from Agroindustrial by-Products as Natural Ingredients for Cosmetics: Chemical Structure and In Vitro Sunscreen and Cytotoxic Activities. *Molecules* **2020**, *25*, 1131.

(20) Alqahtani, M. S.; Alqahtani, A.; Kazi, M.; Ahmad, M. Z.; Alahmari, A.; Alsenaidy, M. A.; Syed, R. Wound-healing potential of curcumin loaded lignin nanoparticles. *J. Drug Delivery Sci. Technol.* **2020**, *60*, No. 102020.

(21) Pang, Y. X.; Sun, Y. N.; Luo, Y. L.; Zhou, M. S.; Qiu, X. Q.; Yi, C. H.; Lou, H. M. Preparation of novel all-lignin microcapsules via interfacial cross-linking of pickering emulsion. *Ind. Crops Prod.* **2021**, *167*, No. 113468.

(22) Chaiyabutr, C.; Sukakul, T.; Kumpangsin, T.; Bunyavaree, M.; Charoenpipatsin, N.; Wongdama, S.; Boonchai, W. Ultraviolet filters in sunscreens and cosmetic products-A market survey. *Contact Dermatitis* **2021**, *85*, 58−68.

(23) Mturi, G. J.; Martincigh, B. S. Photostability of the sunscreening agent 4-tert-butyl-4 '-methoxydibenzoylmethane (avobenzone) in solvents of different polarity and proticity. *J. Photochem. Photobiol., A* **2008**, *200*, 410−420.
(24) Jentzsch, F.; Olsson, O.; Westphal, J.; Reich, M.; Leder, C.; Kummerer, K. Photodegradation of the UV filter ethylhexyl methoxycinnamate under ultraviolet light: Identification and in silico assessment of photo-transformation products in the context of grey water reuse. *Sci. Total Environ.* **2016**, *572*, 1092−1100.
(25) Berenbeim, J. A.; Wong, N. G. K.; Cockett, M. C. R.; Berden, G.; Oomens, J.; Rijs, A. M.; Dessent, C. E. H. Unravelling the Keto-Enol Tautomer Dependent Photochemistry and Degradation Pathways of the Protonated UVA Filter Avobenzone. *J. Phys. Chem. A* **2020**, *124*, 2919−2930.
(26) Karlsson, I.; Hillerstrom, L.; Stenfeldt, A. L.; Martensson, J.; Borje, A. Photodegradation of Dibenzoylmethanes: Potential Cause of Photocontact Allergy to Sunscreens. *Chem. Res. Toxicol.* **2009**, *22*, 1881−1892.
(27) Hanson, K. M.; Narayanan, S.; Nichols, V. M.; Bardeen, C. J. Photochemical degradation of the UV filter octyl methoxycinnamate in solution and in aggregates. *Photochem. Photobiol. Sci.* **2015**, *14*, 1607−1616.
(28) Pattanaargson, S.; Limphong, P. Stability of octyl methoxycinnamate and identification of its photo-degradation product. *Int. J. Cosmet. Sci.* **2001**, *23*, 153−160.
(29) Broadbent, J. K.; Martincigh, B. S.; Raynor, M. W.; Salter, L. F.; Moulder, R.; Sjoberg, P.; Markides, K. E. Capillary supercritical fluid chromatography combined with atmospheric pressure chemical ionisation mass spectrometry for the investigation of photoproduct formation in the sunscreen absorber 2-ethylhexyl-p-methoxycinnamate. *J. Chromatogr. A* **1996**, *732*, 101−110.
(30) Stein, H. V.; Berg, C. J.; Maung, J. N.; O'Connor, L. E.; Pagano, A. E.; MacManus-Spencer, L. A.; Paulick, M. G. Photolysis and cellular toxicities of the organic ultraviolet filter chemical octyl methoxycinnamate and its photoproducts. *Environ. Sci.: Processes Impacts* **2017**, *19*, 851−860.
(31) Lhiaubet-Vallet, V.; Marin, M.; Jimenez, O.; Gorchs, O.; Trullas, C.; Miranda, M. A. Filter-filter interactions. Photostabilization, triplet quenching and reactivity with singlet oxygen. *Photochem. Photobiol. Sci.* **2010**, *9*, 552−558.
(32) Afonso, S.; Horita, K.; Sousa e Silva, J. P.; Almeida, I. F.; Amaral, M. H.; Lobao, P. A.; Costa, P. C.; Miranda, M. S.; Esteves da Silva, J. C.; Sousa Lobo, J. M. Photodegradation of avobenzone: stabilization effect of antioxidants. *J. Photochem. Photobiol., B* **2014**, *140*, 36−40.
(33) Gaspar, L. R.; Campos, P. M. A HPLC method to evaluate the influence of photostabilizers on cosmetic formulations containing UV-filters and vitamins A and E. *Talanta* **2010**, *82*, 1490−1494.
(34) De Vaugelade, S.; Nicol, E.; Vujovic, S.; Bourcier, S.; Pirnay, S.; Bouchonnet, S. UV-vis degradation of alpha-tocopherol in a model system and in a cosmetic emulsion-Structural elucidation of photoproducts and toxicological consequences. *J. Chromatogr. A* **2017**, *1517*, 126−133.
(35) Li, Y. Y.; Yang, D. J.; Lu, S.; Qu, X. Q.; Qian, Y.; Li, P. W. Encapsulating TiO_2 in Lignin-Based Colloidal Spheres for High Sunscreen Performance and Weak Photocatalytic Activity. *ACS Sustainable Chem. Eng.* **2019**, *7*, 6234−6242.
(36) Qiu, X. Q.; Li, Y.; Qian, Y.; Wang, J. Y.; Zhu, S. P. Long-Acting and Safe Sunscreens with Ultrahigh Sun Protection Factor via Natural Lignin Encapsulation and Synergy. *ACS Appl. Bio Mater.* **2018**, *1*, 1276−1285.
(37) Chen, K.; Lei, L.; Qian, Y.; Xie, A. L.; Qiu, X. Q. Biomass Lignin Stabilized Anti-UV High Internal Phase Emulsions: Preparation, Rheology, and Application As Carrier Materials. *ACS Sustainable Chem. Eng.* **2019**, *7*, 810−818.
(38) Bertelli, M.; Kiani, A. K.; Paolacci, S.; Manara, E.; Kurti, D.; Dhuli, K.; Bushati, V.; Miertus, J.; Pangallo, D.; Baglivo, M.; Beccari, T.; Michelini, S. Hydroxytyrosol: A natural compound with promising pharmacological activities. *J. Biotechnol.* **2020**, *309*, 29−33.
(39) Pazos, M.; Alonso, A.; Sanchez, I.; Medina, I. Hydroxytyrosol prevents oxidative deterioration in foodstuffs rich in fish lipids. *J. Agric. Food Chem.* **2008**, *56*, 3334−3340.
(40) Aissa, I.; Kharrat, N.; Aloui, F.; Sellami, M.; Bouaziz, M.; Gargouri, Y. Valorization of antioxidants extracted from olive mill wastewater. *Biotechnol. Appl. Biochem.* **2017**, *64*, 579−589.
(41) Britton, J.; Davis, R.; O'Connor, K. E. Chemical, physical and biotechnological approaches to the production of the potent antioxidant hydroxytyrosol. *Appl. Microbiol. Biotechnol.* **2019**, *103*, 5957−5974.
(42) Guo, W.; An, Y.; Jiang, L.; Geng, C.; Zhong, L. The protective effects of hydroxytyrosol against UVB-induced DNA damage in HaCaT cells. *Phytother. Res.* **2010**, *24*, 352−359.
(43) Maitz, S.; Schlemmer, W.; Hobisch, M. A.; Hobisch, J.; Kienberger, M. Preparation and Characterization of a Water-Soluble Kraft Lignin. *Adv. Sustainable Syst.* **2020**, *4*, No. 2000052.
(44) Sztucki, M.; Narayanan, T. Development of an ultra-small-angle X-ray scattering instrument for probing the microstructure and the dynamics of soft matter. *J. Appl. Crystallogr.* **2007**, *40*, S459−S462.
(45) Wijaya, C. J.; Ismadji, S.; Gunawan, S. A Review of Lignocellulosic-Derived Nanoparticles for Drug Delivery Applications: Lignin Nanoparticles, Xylan Nanoparticles, and Cellulose Nanocrystals. *Molecules* **2021**, *26*, 676.
(46) Toro-Uribe, S.; Ibanez, E.; Decker, E. A.; McClements, D. J.; Zhang, R. J.; Lopez-Giraldo, L. J.; Herrero, M. Design, Fabrication, Characterization, and In Vitro Digestion of Alkaloid-, Catechin-, and Cocoa Extract-Loaded Liposomes. *J. Agric. Food Chem.* **2018**, *66*, 12051−12065.
(47) d'Agostino, S.; Azzali, A.; Casali, L.; Taddei, P.; Grepioni, F. Environmentally Friendly Sunscreens: Mechanochemical Synthesis and Characterization of beta-CD Inclusion Complexes of Avobenzone and Octinoxate with Improved Photostability. *ACS Sustainable Chem. Eng.* **2020**, *8*, 13215−13225.
(48) Vainio, U.; Maximova, N.; Hortling, B.; Laine, J.; Stenius, P.; Simola, L. K.; Gravitis, J.; Serimaa, R. Morphology of dry lignins and size and shape of dissolved kraft lignin particles by X-ray scattering. *Langmuir* **2004**, *20*, 9736−9744.
(49) Trevisan, H.; Rezende, C. A. Pure, stable and highly antioxidant lignin nanoparticles from elephant grass. *Ind. Crops Prod.* **2020**, *145*, No. 112105.
(50) Sayre, R. M.; Dowdy, J. C.; Gerwig, A. J.; Shields, W. J.; Lloyd, R. V. Unexpected photolysis of the sunscreen octinoxate in the presence of the sunscreen avobenzone. *Photochem. Photobiol.* **2005**, *81*, 452−456.
(51) Kikuchi, A.; Yagi, M. Direct observation of the intermolecular triplet−triplet energy transfer from UV-A absorber 4-tert-butyl-4′-methoxydibenzoylmethane to UV-B absorber octyl methoxycinnamate. *Chem. Phys. Lett.* **2011**, *513*, 63−66.

https://doi.org/10.1021/acsomega.2c02133
ACS Omega 2022, 7, 37070−37077